Coupling Charge and Topological Reconstructions at Polar Oxide Interfaces

van Thiel, T.C.; Brzezicki, W.; Autieri, C.; Hortensius, J.R.; Afanasiev, D.; Gauquelin, N.; Jannis, D.; Janssen, N.; Groenendijk, D.J.; Fatermans, J.; Van Aert, S.; Verbeeck, J.; Cuoco, M.; Caviglia, Andrea

How to cite

VAN THIEL, T.C. et al. Coupling Charge and Topological Reconstructions at Polar Oxide Interfaces. In: Physical review letters, 2021, vol. 127, n° 12, p. 127202. doi: 10.1103/PhysRevLett.127.127202

This publication URL: https://archive-ouverte.unige.ch/unige:159303

Publication DOI: 10.1103/PhysRevLett.127.127202

Coupling Charge and Topological Reconstructions at Polar Oxide Interfaces

T. C. van Thiel,[1,*] W. Brzezicki,[2,3] C. Autieri,[2] J. R. Hortensius,[1] D. Afanasiev,[1] N. Gauquelin,[4] D. Jannis,[4] N. Janssen,[1] D. J. Groenendijk,[1] J. Fatermans,[4,5] S. Van Aert,[4] J. Verbeeck,[4] M. Cuoco,[6,7] and A. D. Caviglia[1,†]

[1]*Kavli Institute of Nanoscience, Delft University of Technology, Lorentzweg 1, 2628CJ Delft, Netherlands*
[2]*International Research Centre Magtop, Institute of Physics, Polish Academy of Sciences, Aleja Lotników 32/46, PL-02668 Warsaw, Poland*
[3]*Institute of Theoretical Physics, Jagiellonian University, ulica S. Łojasiewicza 11, PL-30348 Kraków, Poland*
[4]*Electron Microscopy for Materials Science (EMAT), University of Antwerp, Groenenborgerlaan 171, 2020 Antwerp, Belgium*
[5]*Imec-Vision Lab, University of Antwerp, Universiteitsplein 1, 2610 Wilrijk, Belgium*
[6]*SPIN-CNR, IT-84084 Fisciano (SA), Italy*
[7]*Dipartimento di Fisica "E. R. Caianiello", Università di Salerno, IT-84084 Fisciano (SA), Italy*

(Received 11 June 2021; accepted 21 July 2021; published 16 September 2021)

In oxide heterostructures, different materials are integrated into a single artificial crystal, resulting in a breaking of inversion symmetry across the heterointerfaces. A notable example is the interface between polar and nonpolar materials, where valence discontinuities lead to otherwise inaccessible charge and spin states. This approach paved the way for the discovery of numerous unconventional properties absent in the bulk constituents. However, control of the geometric structure of the electronic wave functions in correlated oxides remains an open challenge. Here, we create heterostructures consisting of ultrathin $SrRuO_3$, an itinerant ferromagnet hosting momentum-space sources of Berry curvature, and $LaAlO_3$, a polar wide-band-gap insulator. Transmission electron microscopy reveals an atomically sharp $LaO/RuO_2/SrO$ interface configuration, leading to excess charge being pinned near the $LaAlO_3/SrRuO_3$ interface. We demonstrate through magneto-optical characterization, theoretical calculations and transport measurements that the real-space charge reconstruction drives a reorganization of the topological charges in the band structure, thereby modifying the momentum-space Berry curvature in $SrRuO_3$. Our results illustrate how the topological and magnetic features of oxides can be manipulated by engineering charge discontinuities at oxide interfaces.

DOI: 10.1103/PhysRevLett.127.127202

Recently, an increasing amount of attention has been focused on topological phases in condensed matter [1]. Symmetry is a decisive element, as it can either be essential or detrimental for topological order [2,3]. An iconic example is the quantum Hall effect, where the breaking of time-reversal symmetry is associated with a nonzero Chern number [4]. A second example is the Weyl semimetal, which breaks either time-reversal symmetry, inversion symmetry, or both [5]. Transitions between different topological phases may be achieved through, e.g., external electric or magnetic fields [6–8], a change in chemical composition [9–12], or application of pressure [13–15]. While typically associated with an energy gap, such transitions are not limited to insulators and semimetals. They may also occur in strongly metallic systems [16], which are usually characterized by a high density of interacting electrons [17]. A candidate material is the itinerant ferromagnet $SrRuO_3$ (SRO) [18], which over the past years has been the subject of intense research [19–28]. However, manipulating the properties of SRO-based heterostructures remains an experimental open challenge. Unlike insulators and semimetals, the high carrier density renders electrostatic gating, although possible [21,27,29,30], an inefficient method for manipulating the position of the Fermi level with respect to the momentum-space sources of Berry curvature. This calls for a different approach where the focus lies not on tuning the position of the Fermi level, but rather on changing the topological charges within the Brillouin zone, i.e., inducing a topological transition. In this respect, oxide heterostructures provide an ideal platform due to the strong breaking of inversion symmetry across the interfaces, especially between materials with different charge states [31–34].

In this Letter, we demonstrate control of the momentum-space topological properties of ultrathin SRO, by creating a charge-frustrated interface. We synthesize RuO_2-terminated SRO ultrathin films and interface them with the polar wide-band-gap insulator $LaAlO_3$ (LAO). The charge frustration leads to charge doping of SRO well beyond the capabilities of a conventional electrostatic gate, therefore forming a pronounced profile of excess charge along the growth axis. We then demonstrate that in the ultrathin limit, this charge reconstruction modifies the momentum-space Berry curvature and leads to a full reversal of its sign for all

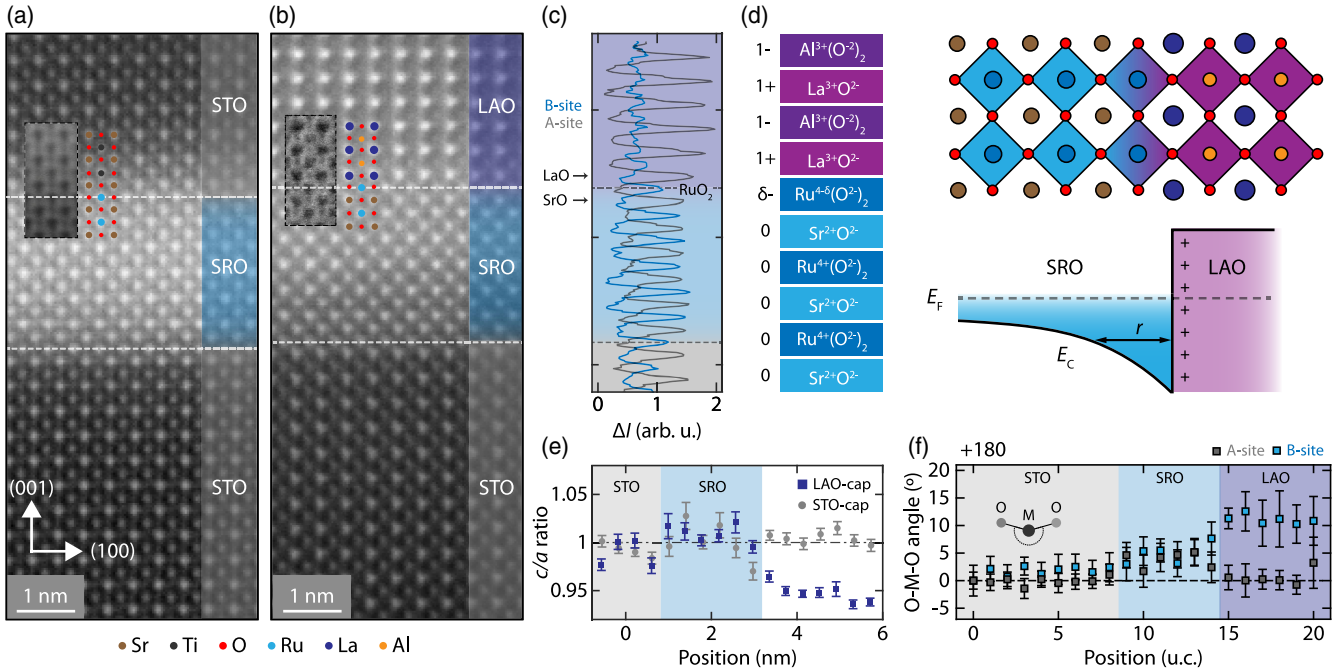

FIG. 1. Atomic characterization. High-angle annular dark-field images of (a) STO/SRO/STO and (b) STO/SRO/LAO heterostructures with the insets showing bright-field images of the interface regions. (c) Intensity profile along the growth axis for the atomic A (gray) and B sites (blue) of (b). (d) Illustration of the charge frustration and the resulting profile of the chemical potential E_C close to the Fermi energy E_F at the LaO/RuO_2 interface. (e) c/a ratio along the growth axis for (a) and (b). (f) O—M—O bond angles for the A and B sites of the STO/SRO/LAO heterostructure, defined with respect to the STO substrate.

temperatures below the magnetic transition, thereby controlling a topological transition in momentum space. These results underline the potential of engineering charge discontinuities at oxide interfaces for inducing topological transitions in correlated matter.

In Figs. 1(a)–1(c), we present scanning transmission electron microscopy data of a nonpolar $SrTiO_3$/SRO/$SrTiO_3$ (STO—SRO—STO) and polar STO—SRO—LAO heterostructure, respectively. Because both STO and SRO have the same Sr A-site cation, the interface between these two ABO_3 perovskites consists of BO_2 layers (B = Ti, Ru) separated by a shared SrO plane. Consequently, both STO and SRO preserve the B^{4+} valence state, and the planar charges are zero on both sides of the interface. In contrast, we find that SRO and LAO are not separated by SrO, but by a shared LaO plane, indicating that the SRO film is RuO_2 terminated. This is a surprising observation since, due to the highly volatile nature of the Ru_xO_y species, the SrO termination has been argued to be more stable in oxidizing conditions [35,36]. The *in situ* stabilization demonstrated here poses a substantial advantage over *ex situ* approaches and is a promising mechanism that invites further exploration [37,38]. Irrespective of its origin, the observed LaO/RuO_2/SrO interface has important consequences for the Ru charge state, with on the SRO side Sr^{2+} requiring Ru^{4+} and on the LAO side La^{3+} requiring Ru^{3+} for charge neutrality. The interface is effectively equivalent to the hybrid compound $Sr_{0.5}La_{0.5}RuO_3$. In a fully ionic picture, charge neutrality is then accomplished by a $Ru^{3.5+}$ charge state, i.e., a $\delta = -0.5e$ excess charge at the interfacial layer [Fig. 1(d)]. Aside from the charge doping, the polarity in the LAO layers creates an attractive electric potential drawing charges toward the interface. Because of the abundance of free carriers in SRO ($n_e \sim 10^{22}$ cm^{-3}), the corresponding electric field is screened over a length r, given approximately by the average distance between free carriers [39]. For our films, this yields $r \approx (n_e)^{-(1/3)} = 5$ Å or 1–2 crystal unit cells. Figure 1(e) shows the out-of-plane unit cell deformation along the growth axis. We find that for both heterostructures, the SRO film, as well as the STO and LAO overlayers, are coherently matched to the in-plane unit cell parameter of the substrate. The mismatch between the unit cell sizes is accommodated through a c-axis elongation in SRO and contraction in LAO [Fig. 1(e)], indicating that the lattice structure is governed by the substrate and not by the capping layer [40]. The absence of antiferrodistortive tilts indicates that the polar field in LAO must be compensated in another manner. In the well-known LAO/STO system, this is accomplished by a polar mode in the LAO layer, where the O—Al—O bonds buckle in response to the internal electric field [41,42], a distortion which propagates into the top few unit cells of the STO substrate. Here, we observe a similar phenomenology, i.e., a polar mode in the LAO layer that propagates into the top unit cell of the SRO layer [Fig. 1(f)].

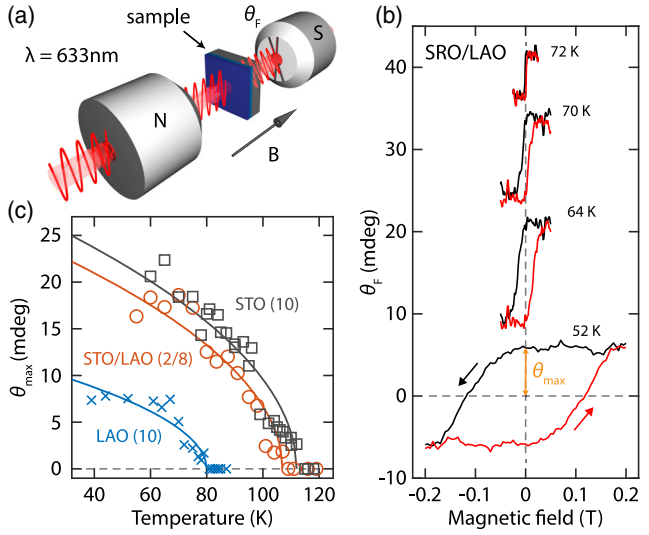

FIG. 2. Magneto-optical Faraday effect. (a) Illustration of the experimental geometry for probing the Faraday rotation. (b) Faraday rotation as a function of applied magnetic field for an SRO(5)/LAO(10) heterostructure for various temperatures. (c) The amplitude of the hysteresis loop $\theta_{\max}$ as a function of applied field for SRO(5)/STO(10) (gray), SRO(5)/STO(2)/LAO(8) (orange), and SRO(5)/LAO(10) (blue) heterostructures. The solid lines represent Landau fits.

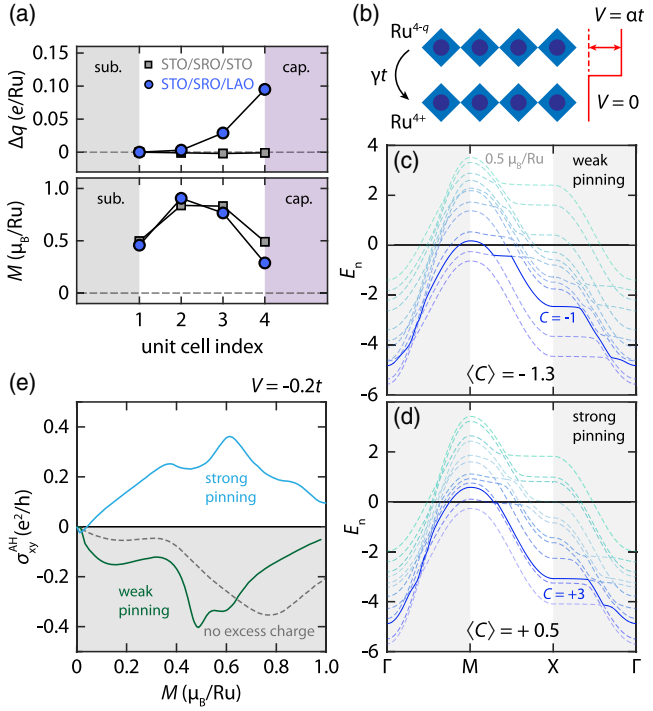

FIG. 3. Excess charge profile and topological reconstruction. (a) Layer-resolved charge and magnetization profile for STO/SRO(4)/STO (gray) and STO/SRO/LAO (blue) calculated using density-functional theory (DFT). (b) Effective tight-binding model of two coupled SRO monolayers, with excess charge $q = -0.5e$ in the top layer, as well as an on site electrostatic potential V and interlayer coupling γt. (c),(d) The 12 Ru t_{2g} bands for the effective model with (c) representing a weak pinning ($\gamma = 1$) and (d) a strong pinning ($\gamma = 0.5$) scenario, including an orbital Rashba correction $\lambda_R = 0.04t$ and an on site potential $V = -0.2t$ in the top layer. (e) The calculated anomalous Hall conductivity $\sigma_{xy}^{\mathrm{AH}}$, in which the gray dashed line represents the reference case with two Ru^{4+} layers ($q = 0$) and the colored solid lines represent the scenarios with excess charge $q = -0.5e$ with either weak (green) or strong pinning (blue).

We next investigate a second consequence anticipated for the excess charge accumulation, i.e., a change in the spin state of the Ru ions. In contrast to some of its magnetic $3d$ counterparts, the crystal-field splitting in SRO (~3 eV) is larger than both the Hund's interaction (~0.3 eV) and the Coulomb repulsion (~2 eV), owing to the spatially larger $4d$ orbitals [43–45]. As a result, the four d electrons in SRO reside in the t_{2g} orbitals, producing a ($4d^4$) $S = 1$ spin state. The additional charge transferred from the LAO layer also occupies the t_{2g} manifold, reducing the average spin state to $3/4 < S_{\mathrm{avg}} < 1$ due to the spin flip. Such a reduction of the spin moment directly manifests in the value of the saturation magnetization M_s and the Curie temperature T_C, which both scale with $S(S+1)$. In magnetic systems, both T_C and M_s can thus serve as indicators of a charge reconstruction and are expected to be lowered when electronic charge is transferred to SRO. We therefore proceed to investigate the spontaneous magnetization as a function of temperature, by means of the magneto-optical Faraday effect [Figs. 2(a) and 2(b)]. The polarization rotation θ_F due to the Faraday effect is linearly proportional to the out-of-plane component of the magnetization M_z. In Fig. 2(c), we show the Faraday rotation as a function of temperature for SRO films with various capping layers. To compare the different M_s and T_C, we fit the data to $\theta = \theta_{T=0}|T - T_C|^{1/2}$ (Landau fit), treating θ as the magnetization M. According to expectation, we find a clear suppression of both T_C and θ_F for the SRO(5)/LAO(10) sample, as compared with SRO(5)/STO(10). To verify that this is an interface-driven effect, we also investigated SRO(5)/STO(2)/LAO(8), which is structurally similar to SRO(5)/LAO(10), but has two layers of STO that shield SRO from the valence discontinuity. As expected, both M_s and T_C are significantly larger compared with the LAO-capped sample and nearly identical to the STO-capped sample, further supporting that the charge and magnetic reconstruction are driven by the charge frustration at the LaO/RuO_2 interface.

Having established an interface-driven charge and spin reconstruction, we turn to the question of how this affects the momentum-space Berry curvature and the anomalous Hall effect (AHE). Aside from the altered magnetization, the charge frustration introduces two elements; (i) a shift in the chemical potential due to charge doping and (ii) breaking of inversion symmetry due to the electric field along the growth axis. To determine their impact, we first address the question of how far the field penetrates into the SRO film.

The top panel in Fig. 3(a) shows the DFT-calculated charge profile across the heterostructure, using the STO substrate as a baseline value. As expected, charge doping is absent for the STO-capped heterostructure, yielding a symmetric charge profile. For the LAO-capped sample however, we find, in accordance with the previous estimate for the screening length r, a doping of ~ -0.1 and $\sim -0.04e$ for the two unit cells closest to the SRO/LAO interface ($\sim 10^{21}$ cm^{-3}), leading to a strongly asymmetric charge profile [46]. The impact on the magnetization is immediately clear from the bottom panel of Fig. 3(a), which, in agreement with the magneto-optical characterization, shows that the two charge-reconstructed unit cells have a lower magnetization compared with the STO/SRO/STO reference case. These results provide a clear picture; the SRO film experiences an electronic and magnetic reconstruction that persists 2 unit cells from the interface and causes a strong inversion-symmetry breaking.

To determine the effect of the reconstruction on the momentum-space Berry curvature, we introduce an effective tight-binding model of an SRO bilayer with interlayer coupling γt, where t is the nearest-neighbour hopping energy [Fig. 3(b)]. The charge frustration and symmetry breaking are simulated by including an additional charge $-0.5e$ in the top layer, an attractive electrostatic potential $V = -0.2t$, and a small orbital Rashba correction $\lambda_R = 0.04t$. The parameter γ represents the tendency of the excess charge being pinned to the top layer, i.e., the screening length r defined in Fig. 1(d). From a band structure perspective, this translates to a steeper bending of the chemical potential E_C near the interface. We consider two scenarios: weak and strong charge pinning, or high and low γ, respectively. Figures 3(c) and 3(d) show the dispersion relations of the twelve Ru t_{2g} bands for the two scenarios, at a representative value of the magnetization. The kinks that can be observed at the band anticrossings represent momentum-space (anti-)vortices of the Berry connection, acting as either positive or negative charges of Berry curvature. We highlight one band as an example, whose Chern number transitions from $C = -1$ to $C = +3$ between the weak and strong pinning scenarios. In the dispersion, this manifests as a change in the position and character of the band anticrossings. Overall, we find a substantial evolution of the topological charges between the two scenarios. One can approximate the total Berry curvature by the averaged Chern number $\langle C \rangle$, which is calculated by summing the Chern numbers of the individual bands, weighted by their occupation. We find a transition of $\langle C \rangle = -1.3$ to $\langle C \rangle = +0.5$, between the weak and strong pinning scenarios, respectively. Concurrently, the filling factors between the two scenarios remain virtually unchanged. In fact, it can be shown that for any linearly decreasing profile of the filling factors with energy, the sign of the total Berry curvature is purely determined by the sum of the Chern numbers associated

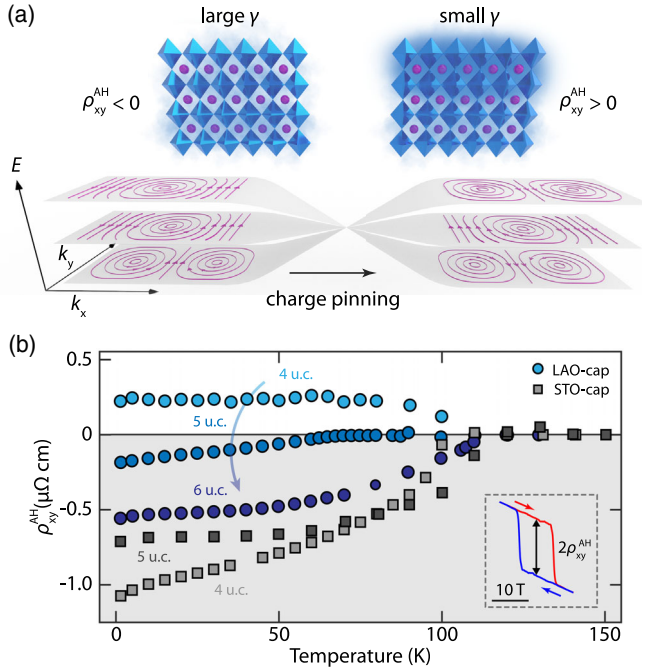

FIG. 4. Anomalous Hall effect. (a) Illustration representing the evolution of the momentum-space topological charges. Upon increasing the charge pinning, the system moves through a Weyl point in the synthetic space spanned by k_x, k_y and the charge pinning parameter γ. (b) The measured anomalous Hall resistivity ρ_{xy}^{AH} for SRO films of varying thickness capped by both STO and LAO as a function of temperature. The inset in (b) shows an example of the magnetic-field dependence of the AHE, from which the amplitude ρ_{xy}^{AH} is extracted.

with the indirect gaps of the twelve t_{2g} bands [47]. This demonstrates that the sign change is driven by a topological transition in momentum-space and is not due to a change in band occupation. To further demonstrate the robustness of this result, we directly calculate the anomalous Hall conductivity for a wide range of values for the magnetization [Fig. 3(e)]. In agreement with the topological charge reconstruction, we find a transition from a fully negative to a fully positive AHE for nearly all magnetization values. These results unambiguously identify the charge pinning, and the resulting inversion-symmetry breaking, as the dominant effect in reconstructing the momentum-space topological charges and Berry curvature.

To illustrate the topological reconstruction, we consider a three-dimensional parameter space, spanned by the Bloch momentum coordinates k_x and k_y and the charge pinning parameter γ as the third dimension. The reconstruction can then be understood as the system moving through a Weyl point, where the bands experience a closing and reopening of an energy gap upon increasing the charge pinning parameter γ. The evolution changes both the number and sign of the topological charges in the two-dimensional Brillouin zone. We have visualized this concept in Fig. 4(a), where the sources of Berry curvature are represented by

chiral vortexlike objects of the Berry connection, which change both in winding direction and in number across the transition. In a transport experiment, this translates to an inversion of the sign of the emergent field and consequently the AHE. Figure 4(b) shows the AHE amplitude, as a function of temperature for films of various thicknesses m capped by STO and LAO. For the thinnest films ($m = 4$), we find a positive AHE for the LAO-capped sample for all temperatures below the T_C. In contrast, it is negative for the 4 u.c. STO-capped sample. These two heterostructures represent the left and right scenarios in Fig. 4(a), and the sign inversion of the AHE can be understood as the system experiencing a topological reconstruction, driven by the onset of charge pinning at the polar interface. As m is increased for the LAO-capped samples, we find a transition to a more negative behavior of the AHE in temperature, which can be understood as the contribution of the charge-reconstructed layers becoming increasingly diluted as the total film thickness increases, effectively diminishing the impact of the interface inversion-symmetry breaking on the anomalous Hall response. Accordingly, one expects both heterostructures to converge to the same state as the number of layers is increased. Indeed, for increasing layer thickness, both heterostructures tend toward the same behavior of the AHE, i.e., a negative at all temperatures.

While electric field penetration in bulk metals can be safely ignored, its importance in the ultrathin limit cannot be neglected. The key element is the extremely short penetration depth of the electrostatic potential in metals, which can cause a strong inversion-symmetry breaking in the near-interface region. The resulting electronic and magnetic reconstructions can have a decisive effect on the momentum-space topological properties of correlated systems, including, but not limited to $SrRuO_3$. The charge frustration arising from the interface with $LaAlO_3$ provides a unique opportunity for studying the effect of symmetry breaking on its momentum-space topology. Because of the insulating nature of $LaAlO_3$, there is neither mixing of states at the Fermi energy nor interface-driven spin canting, as has been reported in, e.g., the $SrRuO_3/SrIrO_3$ interface, which has been the topic of multiple studies in recent years [19,21,26,81,82]. In this sense, the system considered here offers a pleasing simplicity and a more direct approach toward controlling the topology in ultrathin $SrRuO_3$ and potentially other correlated metals. Our results are also of relevance to the scenario of uncapped $SrRuO_3$ films [83], where dangling bonds at the surface can manifest as a charged electrostatic boundary condition [38], albeit complicated by the unavoidable interaction with adsorbed ambient chemical species.

In conclusion, we have demonstrated how a valence charge discontinuity induces both a magnetic and topological reconstruction in ultrathin films of the itinerant ferromagnet $SrRuO_3$. We identify the pinning of the excess charge donated by the polar $LaAlO_3$ overlayer and the resulting inversion-symmetry breaking to be the dominant effect in altering the band topology and momentum-space Berry curvature, leading to a full inversion of the sign of the emergent magnetic field. These results demonstrate how engineering charge discontinuities can be utilized to control the topological properties in oxide heterostructures and establish the potential of interface design toward the manipulation of the geometric structure of wave functions in correlated matter.

The supporting data presented in this Letter are openly available from [84].

The authors thank E. Lesne, M. Lee, H. Barakov, M. Matthiesen, and U. Filippozzi for discussions. The authors are grateful to E. J. S. van Thiel for producing the illustration in Fig. 4(a). This Letter was supported by the European Research Council under the European Unions Horizon 2020 program/ERC Grants No. [677458], No. [770887], and No. [731473] (Quantox of QuantERA ERA-NET Cofund in Quantum Technologies) and by the Netherlands Organisation for Scientific Research (NWO/OCW) as part of the Frontiers of Nanoscience (NanoFront) and VIDI program. The authors acknowledge funding from the European Unions Horizon 2020 research and innovation program under Grant No. [823717]—ESTEEM3. N. G., J. V., and S. V. A. acknowledge funding from the University of Antwerp through the Concerted Research Actions (GOA) project Solarpaint and the TOP project. C. A. and W. B. are supported by the Foundation for Polish Science through the International Research Agendas program cofinanced by the European Union within the Smart Growth Operational Programme. C. A. acknowledges access to the computing facilities of the Interdisciplinary Center of Modeling at the University of Warsaw, Grants No. G73-23 and No. G75-10. W. B. acknowledges support from the Narodowe Centrum Nauki (NCN, National Science Centre, Poland) Project No. 2019/34/E/ST3/00404.

*t.c.vanthiel@tudelft.nl
†a.caviglia@tudelft.nl

[1] J. Wang and S.-C. Zhang, Nat. Mater. **16**, 1062 (2017).
[2] M. Z. Hasan and C. L. Kane, Rev. Mod. Phys. **82**, 3045 (2010).
[3] X.-G. Wen, Rev. Mod. Phys. **89**, 041004 (2017).
[4] F. D. M. Haldane, Phys. Rev. Lett. **61**, 2015 (1988).
[5] A. A. Zyuzin, S. Wu, and A. A. Burkov, Phys. Rev. B **85**, 165110 (2012).
[6] T. Zhang, J. Ha, N. Levy, Y. Kuk, and J. Stroscio, Phys. Rev. Lett. **111**, 056803 (2013).
[7] C.-Z. Chang, J. Zhang, X. Feng, J. Shen, Z. Zhang, M. Guo, K. Li, Y. Ou, P. Wei, L.-L. Wang *et al.*, Science **340**, 167 (2013).
[8] X. Qian, J. Liu, L. Fu, and J. Li, Science **346**, 1344 (2014).

[9] B. A. Bernevig and S.-C. Zhang, Phys. Rev. Lett. **96**, 106802 (2006).
[10] M. König, S. Wiedmann, C. Brüne, A. Roth, H. Buhmann, L. W. Molenkamp, X.-L. Qi, and S.-C. Zhang, Science **318**, 766 (2007).
[11] D. Hsieh, D. Qian, L. Wray, Y. Xia, Y. S. Hor, R. J. Cava, and M. Z. Hasan, Nature (London) **452**, 970 (2008).
[12] P. Dziawa, B. Kowalski, K. Dybko, R. Buczko, A. Szczerbakow, M. Szot, E. Łusakowska, T. Balasubramanian, B. M. Wojek, M. Berntsen *et al.*, Nat. Mater. **11**, 1023 (2012).
[13] X. Xi, C. Ma, Z. Liu, Z. Chen, W. Ku, H. Berger, C. Martin, D. B. Tanner, and G. L. Carr, Phys. Rev. Lett. **111**, 155701 (2013).
[14] T. Liang, S. Kushwaha, J. Kim, Q. Gibson, J. Lin, N. Kioussis, R. J. Cava, and N. P. Ong, Sci. Adv. **3**, e1602510 (2017).
[15] T. Ideue, M. Hirayama, H. Taiko, T. Takahashi, M. Murase, T. Miyake, S. Murakami, T. Sasagawa, and Y. Iwasa, Proc. Natl. Acad. Sci. U.S.A. **116**, 25530 (2019).
[16] X. Ying and A. Kamenev, Phys. Rev. B **99**, 245411 (2019).
[17] D. Pesin and L. Balents, Nat. Phys. **6**, 376 (2010).
[18] Z. Fang, N. Nagaosa, K. S. Takahashi, A. Asamitsu, R. Mathieu, T. Ogasawara, H. Yamada, M. Kawasaki, Y. Tokura, and K. Terakura, Science **302**, 92 (2003).
[19] J. Matsuno, N. Ogawa, K. Yasuda, F. Kagawa, W. Koshibae, N. Nagaosa, Y. Tokura, and M. Kawasaki, Sci. Adv. **2**, e1600304 (2016).
[20] D. Kan, T. Moriyama, K. Kobayashi, and Y. Shimakawa, Phys. Rev. B **98**, 180408(R) (2018).
[21] Y. Ohuchi, J. Matsuno, N. Ogawa, Y. Kozuka, M. Uchida, Y. Tokura, and M. Kawasaki, Nat. Commun. **9**, 213 (2018).
[22] L. Wang, Q. Feng, Y. Kim, R. Kim, K. H. Lee, S. D. Pollard, Y. J. Shin, H. Zhou, W. Peng, D. Lee *et al.*, Nat. Mater. **17**, 1087 (2018).
[23] Z. Li, S. Shen, Z. Tian, K. Hwangbo, M. Wang, Y. Wang, F. M. Bartram, L. He, Y. Lyu, Y. Dong *et al.*, Nat. Commun. **11**, 1 (2020).
[24] T. van Thiel, D. Groenendijk, and A. Caviglia, J. Phys.: Mater. **3**, 025005 (2020).
[25] L. Wang, Q. Feng, H. G. Lee, E. K. Ko, Q. Lu, and T. W. Noh, Nano Lett. **20**, 2468 (2020).
[26] D. J. Groenendijk, C. Autieri, T. C. van Thiel, W. Brzezicki, J. R. Hortensius, D. Afanasiev, N. Gauquelin, P. Barone, K. van den Bos, S. van Aert *et al.*, Phys. Rev. Research **2**, 023404 (2020).
[27] D. Kan, K. Kobayashi, and Y. Shimakawa, Phys. Rev. B **101**, 144405 (2020).
[28] K. Takiguchi, Y. K. Wakabayashi, H. Irie, Y. Krockenberger, T. Otsuka, H. Sawada, S. A. Nikolaev, H. Das, M. Tanaka, Y. Taniyasu *et al.*, Nat. Commun. **11**, 4969 (2020).
[29] S. Shimizu, K. S. Takahashi, M. Kubota, M. Kawasaki, Y. Tokura, and Y. Iwasa, Appl. Phys. Lett. **105**, 163509 (2014).
[30] H. Mizuno, K. T. Yamada, D. Kan, T. Moriyama, Y. Shimakawa, and T. Ono, Phys. Rev. B **96**, 214422 (2017).
[31] N. Reyren, S. Thiel, A. Caviglia, L. F. Kourkoutis, G. Hammerl, C. Richter, C. W. Schneider, T. Kopp, A.-S. Rüetschi, D. Jaccard *et al.*, Science **317**, 1196 (2007).
[32] A. Tsukazaki, A. Ohtomo, T. Kita, Y. Ohno, H. Ohno, and M. Kawasaki, Science **315**, 1388 (2007).
[33] H. Y. Hwang, Y. Iwasa, M. Kawasaki, B. Keimer, N. Nagaosa, and Y. Tokura, Nat. Mater. **11**, 103 (2012).
[34] E. Skoropata, J. Nichols, J. M. Ok, R. V. Chopdekar, E. S. Choi, A. Rastogi, C. Sohn, X. Gao, S. Yoon, T. Farmer *et al.*, Sci. Adv. **6**, eaaz3902 (2020).
[35] G. Rijnders, D. H. Blank, J. Choi, and C.-B. Eom, Appl. Phys. Lett. **84**, 505 (2004).
[36] G. Koster, L. Klein, W. Siemons, G. Rijnders, J. S. Dodge, C.-B. Eom, D. H. Blank, and M. R. Beasley, Rev. Mod. Phys. **84**, 253 (2012).
[37] J. Shin, S. Kalinin, H. Lee, H. Christen, R. Moore, E. Plummer, and A. Baddorf, Surf. Sci. **581**, 118 (2005).
[38] H. G. Lee, L. Wang, L. Si, X. He, D. G. Porter, J. R. Kim, E. K. Ko, J. Kim, S. M. Park, B. Kim, A. Thye Shen Wee, A. Bombardi, Z. Zhong, and T. W. Noh, Adv. Mater. **32**, 1905815 (2020).
[39] J. C. Slater, Phys. Rev. **81**, 385 (1951).
[40] This is further substantiated by a strong suppression of the octahedral tilts, yielding a tetragonal lattice symmetry, see Section I.B of the Supplemental Material.
[41] M. Huijben, A. Brinkman, G. Koster, G. Rijnders, H. Hilgenkamp, and D. H. Blank, Adv. Mater. **21**, 1665 (2009).
[42] J. Gazquez, M. Stengel, R. Mishra, M. Scigaj, M. Varela, M. Roldan, J. Fontcuberta, F. Sánchez, and G. Herranz, Phys. Rev. Lett. **119**, 106102 (2017).
[43] J. Lee, Y. Lee, T. Noh, K. Char, J. Park, S.-J. Oh, J.-H. Park, C. Eom, T. Takeda, and R. Kanno, Phys. Rev. B **64**, 245107 (2001).
[44] M. S. Laad and E. Müller-Hartmann, Phys. Rev. Lett. **87**, 246402 (2001).
[45] H. T. Dang, J. Mravlje, A. Georges, and A. J. Millis, Phys. Rev. B **91**, 195149 (2015).
[46] Note that the charges do not add up to −0.5e due to the covalent bonding between ions considered in DFT i.e., a considerable portion of the additional charge resides in the interstitial space and oxygen ligands.
[47] See Supplemental Material at http://link.aps.org/supplemental/10.1103/PhysRevLett.127.127202 for additional data and further details regarding the synthesis, structural characterization, theoretical calculations, transport measurements, sample synthesis, STEM characterization, magnetic characterization, and theoretical analysis, and which includes Refs. [48–80].
[48] C. Lichtensteiger, J. Appl. Crystallogr. **51**, 1745 (2018).
[49] W. Gordy and W. O. Thomas, J. Chem. Phys. **24**, 439 (1956).
[50] E. K. Ko, J. Mun, H. G. Lee, J. Kim, J. Song, S. H. Chang, T. H. Kim, S. B. Chung, M. Kim, L. Wang *et al.*, Adv. Funct. Mater. **30**, 2001486 (2020).
[51] N. Gauquelin, K. Van den Bos, A. Béché, F. Krause, I. Lobato, S. Lazar, A. Rosenauer, S. Van Aert, and J. Verbeeck, Ultramicroscopy **181**, 178 (2017).
[52] S. Findlay, N. Shibata, H. Sawada, E. Okunishi, Y. Kondo, T. Yamamoto, and Y. Ikuhara, Appl. Phys. Lett. **95**, 191913 (2009).
[53] A. De Backer, K. Van den Bos, W. Van den Broek, J. Sijbers, and S. Van Aert, Ultramicroscopy **171**, 104 (2016).
[54] J. Fatermans, A. den Dekker, K. Müller-Caspary, N. Gauquelin, J. Verbeeck, and S. Van Aert, Ultramicroscopy **219**, 113046 (2020).

[55] E. Breckenfeld, R. Wilson, J. Karthik, A. R. Damodaran, D. G. Cahill, and L. Martin, Chem. Mater. **24**, 331 (2012).
[56] Y. J. Chang, C. H. Kim, S.-H. Phark, Y. S. Kim, J. Yu, and T. W. Noh, Phys. Rev. Lett. **103**, 057201 (2009).
[57] M. E. Fisher and J. Langer, Phys. Rev. Lett. **20**, 665 (1968).
[58] J. H. Cho, Q. X. Jia, X. D. Wu, S. R. Foltyn, and M. P. Maley, Phys. Rev. B **54**, 37 (1996).
[59] D. Kim, B. L. Zink, F. Hellman, S. McCall, G. Cao, and J. E. Crow, Phys. Rev. B **67**, 100406(R) (2003).
[60] M. Kim and B. I. Min, Phys. Rev. B **91**, 205116 (2015).
[61] G. Kresse and J. Furthmüller, Comput. Mater. Sci. **6**, 15 (1996).
[62] G. Kresse and J. Furthmüller, Phys. Rev. B **54**, 11169 (1996).
[63] J. P. Perdew and A. Zunger, Phys. Rev. B **23**, 5048 (1981).
[64] D. M. Ceperley and B. J. Alder, Phys. Rev. Lett. **45**, 566 (1980).
[65] C. Autieri, J. Phys. Condens. Matter **28**, 426004 (2016).
[66] P. E. Blöchl, O. Jepsen, and O. K. Andersen, Phys. Rev. B **49**, 16223 (1994).
[67] T. A. Manz and N. G. Limas, RSC Adv. **6**, 47771 (2016).
[68] A. Liechtenstein, V. I. Anisimov, and J. Zaanen, Phys. Rev. B **52**, R5467 (1995).
[69] C. Etz, I. V. Maznichenko, D. Böttcher, J. Henk, A. N. Yaresko, W. Hergert, I. I. Mazin, I. Mertig, and A. Ernst, Phys. Rev. B **86**, 064441 (2012).
[70] N. Marzari and D. Vanderbilt, Phys. Rev. B **56**, 12847 (1997).
[71] I. Souza, N. Marzari, and D. Vanderbilt, Phys. Rev. B **65**, 035109 (2001).
[72] A. A. Mostofi, J. R. Yates, Y.-S. Lee, I. Souza, D. Vanderbilt, and N. Marzari, Comput. Phys. Commun. **178**, 685 (2008).
[73] S. G. Jeong, T. Min, S. Woo, J. Kim, Y.-Q. Zhang, S. W. Cho, J. Son, Y.-M. Kim, J. H. Han, S. Park *et al.*, Phys. Rev. Lett. **124**, 026401 (2020).
[74] C. Autieri, M. Cuoco, and C. Noce, Phys. Rev. B **89**, 075102 (2014).
[75] R. Karthikeyan and M. K. Niranjan, IEEE Trans. Magn. **54**, 1 (2018).
[76] R. Pentcheva, R. Arras, K. Otte, V. G. Ruiz, and W. E. Pickett, Phil. Trans. R. Soc. A **370**, 4904 (2012).
[77] P. Mori-Sánchez, A. J. Cohen, and W. Yang, Phys. Rev. Lett. **100**, 146401 (2008).
[78] G. Khalsa, B. Lee, and A. H. MacDonald, Phys. Rev. B **88**, 041302(R) (2013).
[79] M. Malvestuto, E. Carleschi, R. Fittipaldi, E. Gorelov, E. Pavarini, M. Cuoco, Y. Maeno, F. Parmigiani, and A. Vecchione, Phys. Rev. B **83**, 165121 (2011).
[80] H. Jeong, S. G. Jeong, A. Y. Mohamed, M. Lee, W.-s. Noh, Y. Kim, J.-S. Bae, W. S. Choi, and D.-Y. Cho, Appl. Phys. Lett. **115**, 092906 (2019).
[81] B. Pang, L. Zhang, Y. Chen, J. Zhou, S. Yao, S. Zhang, and Y. Chen, ACS Appl. Mater. Interfaces **9**, 3201 (2017).
[82] Z. Zeng, J. Feng, X. Zheng, C. Wang, J. Liu, Z. Lu, F.-X. Jiang, X.-H. Xu, Z. Wang, and R.-W. Li, Appl. Phys. Lett. **116**, 142401 (2020).
[83] Y. Gu, Y.-W. Wei, K. Xu, H. Zhang, F. Wang, F. Li, M. S. Saleem, C.-Z. Chang, J. Sun, C. Song *et al.*, J. Phys. D **52**, 404001 (2019).
[84] T. C. van Thiel, W. Brzezicki, C. Autieri, J. Hortensius, D. Afanasiev, N. Gauquelin, D. Jannis, N. Janssen, D. Groenendijk, J. Fatermans, S. van Aert, J. Verbeeck, M. Cuoco, and A. Caviglia, Coupling charge and topological reconstructions at polar oxide interfaces, https://doi.org/10.5281/zenodo.4552830.